https://doi.org/10.5194/egusphere-2026-2921
Preprint. Discussion started: 8 July 2026

UAP Orbs: Magnetically Confined Dusty Plasmoids Produced by Meteors

John W. Birks[1]

[1]Department of Chemistry, University of Colorado, Boulder, Colorado, 80309, USA
Correspondence to: John W. Birks (birks@colorado.edu)

Abstract. One of the most commonly reported Unidentified Anomalous Phenomena (UAP) is a large, bright, luminescent sphere observed in the lower troposphere and colloquially referred to as an "orb." Analysis of 508 orb sightings reported to the National UFO Reporting Center (NUFORC) indicates that these silent, floating luminous objects often exhibit plasma-like behavior and emit visible light of varying colors for durations of up to an hour or more. In this work, citizen-science reports of orb observations are shown to be significantly correlated (~3σ) with reports of meteor fireballs, suggesting a meteoritic origin. We propose that some orbs may represent a previously unrecognized type of weakly ionized dusty plasma formed by stabilization of meteoric dust in the lower atmosphere. A preliminary physical model is presented in which remanent magnetization of meteoritic particles, particularly elemental iron, nickel, and magnetite, contributes to aggregation and confinement of the dust cloud. In this hypothesis, heat from the oxidation of metallic iron and nickel provides an energy source and facilitates thermal buoyancy, while electrical activity arises from triboelectric charging driven by particle collisions and convective mixing. The wide range of reported orb colors is broadly consistent with microdischarges in air and emissions from pyrophoric combustion of iron- and nickel-containing particles. Because iron meteorites and the iron–nickel components of ordinary stony meteorites can survive atmospheric entry into the lower atmosphere, meteoritic material may provide a natural explanation for orb observations.

1 Introduction

Luminous spheres in the atmosphere, colloquially known as "orbs," are one of the most frequently reported types of Unidentified Anomalous Phenomena (UAP), with hundreds of reports of orb observations filed each year. This paper includes a partial review of citizen reports of glowing orbs filed online with the National UFO Reporting Center (NUFORC, 2026). Those reports, which include written descriptions, photos and videos, provide insight useful in formulating a plausible theory of the physics of orb formation and behaviour. Some characteristics of orbs that need to be explained include: (1) an adequate source of energy to provide buoyancy, electrical activity and light emission; (2) a means of confining the glow to an approximate sphere; (3) long life of up to an hour or more, (4) visible emission over a wide spectral range, sometimes changing colours or flashing different colours; (5) a corona with electrical discharges into surrounding air; (6) frequent observations of many orbs traveling together; (7) weak binding of two or more orbs with "bond lengths" of up to ~1-2 orb diameters; (8) merging of orbs and splitting of orbs to form two or more orbs; (9) blinking on and off of orb emissions; and (10) glowing orbs inducing emissions from nearby dark orbs.

https://doi.org/10.5194/egusphere-2026-2921
Preprint. Discussion started: 8 July 2026

Following a survey of reported orb observations, a preliminary theory is proposed here that accounts for all these properties. In this theory, orbs are derived from meteoric dust that stabilizes in the lower atmosphere. Iron plays a central role in this theory, providing both containment of the orb through remanent magnetization and energy through its highly exothermic oxidation. It is proposed that the observed electrical activity is derived from the triboelectric effect, with visible light emission arising from both electrical discharge in air and combustion of iron and nickel nanoparticles.

2 Analysis of luminous orb data reported on the National UFO Reporting Center (NUFORC) website

NUFORC provides an online means for individuals to provide reports of observations of what formerly were known as Unidentified Flying Objects (UFOs) and are now referred to by the U.S. Government as Unidentified Anomalous Phenomena (UAP). Reports are made online and available to the public since the launch of their website in 1995. To date, more than 160,000 reports have been filed online. Reports consist of date, time, duration and location of observation, colour, number and shape of the UAP, speed of movement and many other factors. Importantly, a small fraction of reports includes uploaded photos and videos. The presence of media makes it possible to attribute many observations to known phenomena such as planets, stars, rockets, meteors, sky lanterns, etc. Because a large fraction of reports can be attributed to natural or other phenomena unrelated to orbs, we limited our study to reports with imagery. Also, due to limited reports in early years, data analysed here are confined to the inclusive period 2000-2025. During this period, 1,296 reports responding to the search term “orb” contained photos and/or videos. Those reports were examined in random order and either accepted or rejected as likely being reports of luminous orbs--defined simply as unexplained glowing spheres of light in the sky. Minimal criteria for acceptance were (1) having credible imagery, (2) observation of luminance (therefore almost entirely nighttime) of an object in the sky and (3) no associated solid structures. Reports included annotations by NUFORC of many sitings likely being balloons, aircraft, drones, rockets (with specific launch dates), sky lanterns, planets, meteors, stars, the moon, space junk, Starlink, the International Space Station, searchlights, birds, insects, camera anomalies, etc. The final assessment generally agreed with NUFORC except in the instance of sky lanterns, which were mostly reassigned as orbs. Additionally, observations were rejected in cases of (1) narrative statements that the reported phenomena occur frequently, (2) regular blinking of red and/or green lights at ~1 Hz indicative of drones or aircraft, and (3) sudden acceleration suggestive of drones. The goal was to reduce the data set to those most likely to represent a single class of UAP (referred to here as “orbs”) with similar characteristics such that observations could be further analysed for correlations with other parameters such as fireball observations, periods of meteor showers, meteorological parameters, etc. Examination of the reports also revealed observations of orbs in associations with meteors, as further addressed below. Of the reports examined, 508 (39%) were accepted as likely observations of orbs for this study, of which 408 were observations made in the US.

https://doi.org/10.5194/egusphere-2026-2921
Preprint. Discussion started: 8 July 2026

2.1 Characteristics of the orb class of UAP

2.1.1 Shape, size and colour

The most often reported orb is a bright white or bluish white sphere, observed to be as bright or brighter than Venus and larger by a factor of several diameters. Many are a yellowish white, while others are orange or even bright red. A few are blue or green. Many observers report that orbs flicker or sparkle in one or more colours, including all colours of the rainbow, and many report that the orb is surrounded by a corona. Estimated sizes range from that of a basketball to that of a house or even larger, but often there is no estimate of size because of a lack of a reference point against the dark sky. The median reported size is approximately in the range of 1-3 m. Orbs occur singly, but about as often with one or more additional orbs of varying sizes, brightnesses and sometimes colours. Observers often report that orbs continuously change shape but on average are spherical. Examples of seven orb photos, some from video frames, are provided in Fig. 1.

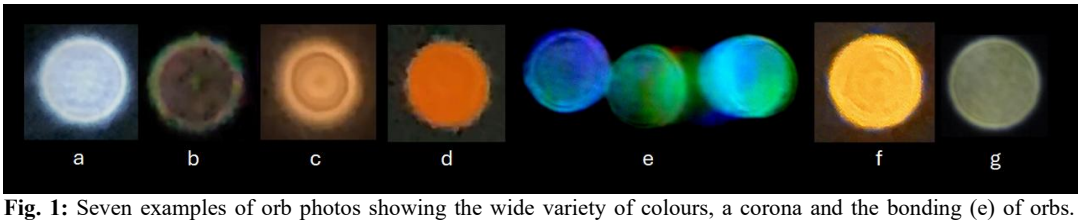

Fig. 1: Seven examples of orb photos showing the wide variety of colours, a corona and the bonding (e) of orbs. NUFORC siting reports for individual images are a (192492), b (185621), c (185625), d (182271), e (168160), f (183903), and g (179226).

A fuzzy, thin corona that is ~5-15% of the orb diameter is apparent in nearly all of these photos, and what appear to be multicoloured microdischarges from the surface are best seen in the video associated with Fig. 1b (NUFORC report 185621). (Note that the hyperlinks for NUFORC reports are https://nuforc.org/sighting/?id=xxxxxx where "xxxxxx" is the report number. Observational details, a narrative description of the event, and additional images and videos can be viewed on the report webpages.) Figure 1e shows contact and longer distance bonding of three blue and green orbs (NUFORC report 168160). It should be kept in mind that nearly all photos and videos were obtained with smart phone cameras, which are known to have associated artifacts due to optics, autoexposure, autofocus, image processing, and spread of images of distant objects over a small number of pixels that affect shape, colour and other image properties But many aspects like flickering of colours, changes in shape and coronas were often reported as being confirmed by direct unassisted visual observation and by using scopes and binoculars. Orbs are observed to persist for times ranging from a few minutes to several hours. Often, they just blink out, possibly explaining some reports that they sped away at incredible speeds. They make no audible sound and typically move slowly. Observers sometimes report that one or more orbs moved against the wind, but wind direction often changes with altitude. It is more likely that orbs simply move with the wind, sometimes rising and sinking due to internal temperature changes.

https://doi.org/10.5194/egusphere-2026-2921
Preprint. Discussion started: 8 July 2026

2.1.2 Plasma-like behaviour

The above-mentioned descriptions are suggestive of orbs being confined plasmas. Indeed, some observers use the terms “plasma” or “plasmoid” when describing such phenomena in their reports. Plasma-based interpretations of UAPs in the thermosphere and near-Earth space have been proposed recently (Joseph et al., 2024a,b; Joseph et al., 2025). The present study addresses persistent luminous orb phenomena observed in the lower troposphere, where pressures are many orders of magnitude higher and high-energy radiation is generally unavailable to sustain significant ionization. As in the work of Joseph et al., some of the strongest evidence for plasma-like behaviour arises from photographic and video observations of multiple luminous objects that appear to interact with one another through coordinated motion and other complex behaviours. There are reports of orbs splitting into two or more orbs (e.g., NUFORC reports 183546 and 194306) and of two orbs combining into a single orb. A single orb sometimes has one or more satellite orbs that appear to be captured in its electric field such that they move together. A good example of some of these behaviours is shown in Fig. 2, which contains cropped frames of a video where two orbs approach each other and reorganize into an agglomerate of three orbs.

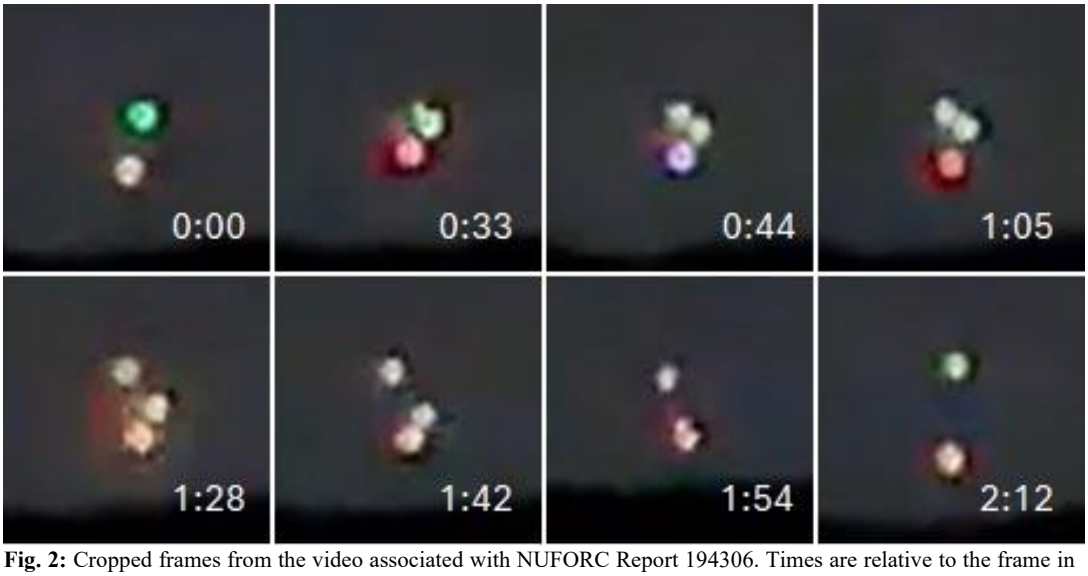

Fig. 2: Cropped frames from the video associated with NUFORC Report 194306. Times are relative to the frame in the upper left corner. Video obtained on 22 Nov 2025 at 20:10 local time in the Estrella Mountains outside of Gila Bend, AZ.

This agglomerate then splits off one orb, followed by the remaining two orbs merging (best seen in the video) (NUFORC report 194306). Note that the colours of different orbs vary from frame to frame, and when the orbs are close, there is a reddish-brown glow that appears to be light scattering from the interstitial space (possibly from meteoric dust, discussed below, being exchanged or lost). In some cases, orbs suddenly appear and disappear as suggestive of plasma ignition and quenching (NUFORC report 178910). Some orbs flash at a very fast rate similar to the flicker of a fluorescent light with defective ballast (NUFORC report 179425; in this report showing rapid blinking, what appear to be in-phase multiple orbs could be due to an artifact of viewing through a multi-paned window). These observations are strongly indicative of plasma behaviour. If orbs are dusty (complex) plasmas (Merlino, 2021; Morfill,

https://doi.org/10.5194/egusphere-2026-2921
Preprint. Discussion started: 8 July 2026

G. E. and Ivlev, 2009), the weak binding of two or more orbs, as seen in Fig. 1e and Fig. 2, would be expected due to charge-induced dipole, dipole-dipole and other multipole electrostatic interactions associated with non-uniform internal charge distributions. Magnetic dipole attractions between orbs also would be expected at close range and could contribute to orb binding if they contain magnetized particles as discussed below.

3 Coincidence of observations of orbs and meteors

Fireballs are bright meteors conventionally defined as appearing brighter than Venus. The American Meteor Society (AMS) maintains a citizen-science database of fireball observations, in which multiple individual reports are grouped into single fireball events, each event being characterized by time and location (American Meteor Society, 2026). The database is searchable by country and U.S. state, enabling geographically constrained comparisons.

3.1 Temporal correlation of orb and fireball observations

To test for a correlation between orb sightings reported to NUFORC and fireball observations reported to the AMS, the fireball database was searched for events occurring within 3 h before or 4 hours after each orb observation. Matches were binned into seven 1-h intervals. To minimize heterogeneity in reporting practices and observational bias, the analysis was restricted to U.S. states, where the vast majority of both orb and fireball reports originate from amateur observers using similar observational platforms. During the inclusive period 2020–2025, a total of 408 U.S. orb observations meeting the selection criteria described above were identified. Of these, 94 coincided with at least one AMS fireball report in the same state during the 3 hours before an orb observation and 4 hours after (Fig. 3).

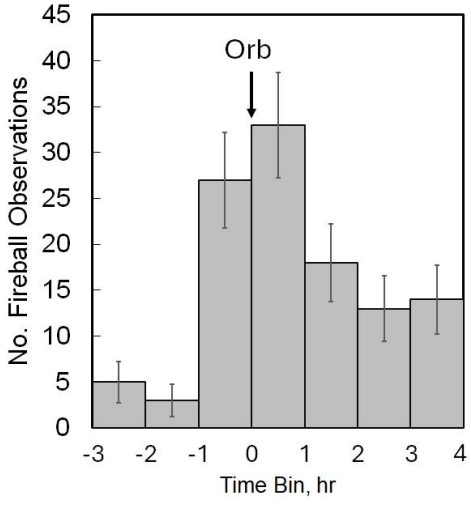

Fig. 3: Number of fireball events occurring within 1-hr periods relative to observation of an orb in that state. Bin 0-1 represents the 1-hr period following observation of an orb. Error bars are 1σ.

https://doi.org/10.5194/egusphere-2026-2921
Preprint. Discussion started: 8 July 2026

The temporal distribution of these coincidences is strongly peaked near the time of orb observation: 60 fireballs occurred within ±1 h of an orb observation, compared with 8 fireballs during the 2 preceding hours (−3 to −1 h) and 45 fireballs during the 3 following hours (+1 to +4 h). If bright fireballs were isolated, singular events, correlations with orb observations would be expected primarily, if not exclusively, during the ~1 h interval immediately preceding an orb report. Instead, comparable excesses of fireball reports are observed both before and after orb sightings. This temporal symmetry is inconsistent with a one-to-one causal association between a single detected fireball and a subsequent orb observation. However, this pattern can be explained by the well-established tendency for meteoroids to arrive in temporally clustered groups rather than as isolated events (Jenniskens, 1995; Jenniskens et al., 2016). Fine-scale structure within meteoroid streams—such as dust trails and filaments—produces enhanced meteor activity over timescales of tens of minutes to several hours (Vaubaillon et al., 2005; Rendtel, 2014). Because only a small fraction of meteoroid entries is detected and reported, an observed fireball frequently serves as a proxy for multiple nearby meteoroid entries, including additional fireballs that may have occurred earlier or later but went unobserved. Under these conditions, observed orb–fireball coincidences extending 1–2 h both before and after an orb report are expected.

3.1.1 Estimation of the random background coincidence rate

In order to assess statistical significance, it is necessary to establish the expected background rate of random orb–fireball coincidences. A naïve comparison between the ±1 h bins and more distant bins yields an apparent excess at very high confidence ($Z \approx 5$), but this approach does not account for strong time-of-day variations in observational efficiency. Both orbs and fireballs are more frequently observed during the early nighttime hours, particularly within ~1–2 h after sunset when it is sufficiently dark but citizen observers are not sleeping. Also, a substantial fraction of the −3 to −2 h and −2 to −1 h bins fall during daylight, artificially suppressing the apparent background rate due to poor visibility.

To remove time of day as a confounding variable, we therefore compared fireball counts during the ±1 h window surrounding each orb observation with fireball counts during the same local time windows on the day before and the day after each orb observation. Results from both analyses are summarized in Table 1.

Table 1. Numbers of fireballs reported relative to times of orb sightings.

	Time Relative to Orb Sighting, hr						
	-3 to -2	**-2 to -1**	**-1 to 0**	**0 to 1**	**1 to 2**	**2 to 3**	**3 to 4**
Day before			18	14			
Day of	5	3	27	33	18	13	14
Day after			18	21			

From the day-before and day-after comparisons, we estimate the random background rate of coincidental orb and fireball sightings to be 17.8 ± 2.9**.** This value is consistent with the 18 fireballs observed in the 1 to 2 h bin vin on the actual day of orb sightings and is modestly higher than the 13 and 14 fireballs observed in subsequent hours. In

https://doi.org/10.5194/egusphere-2026-2921
Preprint. Discussion started: 8 July 2026

contrast, only 3 and 5 fireballs were observed in the -2 to -1 and -3 to -2 periods, respectively, on the same day of orb observation, reflecting an observational bias of fireballs during those periods, many of which are during daylight hours.

An independent estimate of the average background rate can be obtained from the overall AMS fireball statistics. In 2025, 10,443 fireball events were reported over 4,380 daylight hours across 51 U.S. states and districts, corresponding to an average probability of 0.0467 for observing a fireball in any given state during any single hour. For 408 orb observations, this implies an expected 19.1 random orb–fireball coincidences per 1-h interval. When weighted by the distribution of fireball and orb reports over the full 2020–2025 period, the expected background becomes 17.1, in excellent agreement with the 17.8 ± 2.9 value derived from the day-before/day-after analysis.

3.1.2 Statistical significance

The significance of the excess fireball rate during the orb ±1 h window relative to the background rates on the day before and day after orb observation is most appropriately evaluated using a conditional binomial test. The null hypothesis is that the fireball rate during the orb's ±1 h window is identical to the rate at the same local times on adjacent days. A total of 60 fireballs were observed during the orb ±1 h window ($T_1 = 2$ h), while a total of 72 fireballs were observed during the corresponding windows on the day before and day after ($T_2 = 4$ h), yielding a total of n = 132 fireballs. Under the null hypothesis, the expected number during the orb window is E = pn, where $p = T_1/(T_1 + T_2) = 1/3$, giving E = 44. The variance is

$$\sigma^2 = np(1-p) = 132 \times \frac{1}{3} \times \frac{2}{3} = 29.3, \quad (1)$$

and thus σ = 5.42. The resulting Z-score is Z = (60 − 44)/5.42 = 2.95. A Poisson rate-ratio test yields a consistent value of Z = 2.99. Thus, the null hypothesis can be rejected with >99% confidence (one-sided p ≈ 0.003; two-sided p ≈ 0.006), demonstrating a highly significant statistical correlation between orb observations and enhanced fireball activity.

3.1.3. Direct reports of orb and meteor associations

There are several submitted reports, as summarized in Table 2, of observations of orbs almost immediately following observation of a meteor. These eyewitness observations reinforce results of the statistical analysis presented above that demonstrates a strong correlation of orb and fireball observations by independent observers.

Table 2. NUFORC reports of meteors becoming orbs.

Observation	NUFORC Report No.[a]
"I … turned to look into the night sky and see a light blue what I thought was a comet falling from the sky. It started turning and dimmed down to an orb." The report includes a video of a bright white orb. (2023-04-03, 20:38 Local, Fort Worth, TX).	177770

https://doi.org/10.5194/egusphere-2026-2921
Preprint. Discussion started: 8 July 2026

"The sighting occurred shortly after I observed the largest and brightest falling star I have ever seen. Moments after the meteor disappeared, two glowing orange orbs appeared in the sky." The report contains a video showing two orbs. (2024-12-30, 21:21 Local, Hereford, TX).	187380
"I was ready to leave my driveway around 8 pm on Saturday September 16, 2023 and was startled to observe a short flash, very defined light burst where I looked up to the left in the dark sky, which appeared similar to a falling star but much shorter and wider, and probably a mile high. It then stopped and turned into a round bright light." The two reports include a video of an orb and two photos. (2023-9-16, 20:00 Local, Levittown, NY).	178308 179172
"… I noticed a bright light emerging high in the sky. At first, it appeared to be a meteor plummeting into the atmosphere with a fairly straight downward trajectory. It looked small but noticeable, burning with a bright red-orange glow. … Its descent eventually came to a stop just above the cloud line, and then it started moving back and forth—side to side—without changing altitude. The object continued to emit light, appearing to radiate from itself." Still photos show an orange orb. (2025-04-01, 21:40 Local, Tacoma, WA).	189721
"Shortly after noticing what appeared to be an asteroid, I observed a separate object enter my field of view from the north and travel smoothly toward the south. The object was completely silent and moved at a steady, controlled pace." (2025-12-14, 00:48 Local, Albuquerque, NM).	194726

.

One other report (NUFORC Report 192338) provided continuous video of what appeared to be a meteor transitioning into an orb. However, based on angle of entry and the long entry time of greater than 40 s, (meteor entries typically occur in less than 1s), this video is almost certainly the re-entry of the Genesis 2 experimental space habitat (NORAD ID 31789), which was deorbited within a few minutes of the reported observation time (N2YO, 2026). The video is very useful, however, in showing how a mass entering the atmosphere can form a stabilized glowing sphere (Fig. 4) that persists for at least 1 min. Whether this object became a long-lived orb is unknown. There probably aren't enough orbital re-entries, 820 re-entries in 2025 (Aerospace Corporation, 2026), to account for the number of reported orb observations due to most being controlled to fall over open oceans, but it is possible that they contribute to orb formation. Satellites are composed mostly of aluminium, but booster rockets contain large amounts of iron, which, as hypothesized below, is required for orb formation.

The high correlation between orb and meteor observations in combination with eyewitness reports leads to the hypothesis that orbs are derived from impacts of some subset of meteors that reach the troposphere. The remainder of this paper addresses the difficult questions of how orbs formed from the remnants of meteors could remain intact, be buoyant, exhibit plasma-like behaviour and emit electromagnetic energy for up to several hours.

https://doi.org/10.5194/egusphere-2026-2921
Preprint. Discussion started: 8 July 2026

Fig. 4: Re-entry of Genesis 2 experimental space habitat. Frame captures from video of NUFORC Report 192238. Upper image at time ~20 s. Lower image is of the luminescent semi-stabilized remnant at ~51 s. In the video, light emission from the fireball extinguishes at time ~41 s, then reappears much bright at ~50 s.

3.1.4 Frequencies of meteor impacts

The frequency of meteoroid impacts with the atmosphere are many orders of magnitude more frequent than required to account for the rate of orb observations. A widely used empirical normalization for the cumulative number of impacts N on the atmosphere by meteoroids in the size range of millimetres to meters is given by

$$N(>D) \approx 3.7 \times 10^{7}\ D^{-2.7} \quad (2)$$

where D is the diameter in meters (Brown et al., 2002). Table 2 shows the estimated number of meteoroid impacts in the size range 1 cm to 1 m per year. The fraction of orbs being reported by people is likely extremely low due to most (>95%) of the surface area of Earth being uninhabited, meteors being noticeable primarily at night while most people remain indoors, only a small fraction of orbs being bright enough to see, and only a small fraction of observers filing reports. As discussed below, meteors reaching the troposphere and forming observable orbs are likely to be only a few to a few tens of centimetres in diameter. Considering that only a small fraction of meteors might form orbs, and with less than one reported orb observation per day, there are enough impacts, for example, to allow a combined meteor-to-orb conversion, observation, and reporting efficiency of less than less than 2.0×10^{-8} for a 10-cm meteoroid or 1.5×10^{-6} for a 50-cm meteoroid. Thus, only a tiny fraction of impacts is required to have a "Goldilocks" combination of size, composition, velocity, impact angle and other properties to produce an observed orb.

Table 2. Approximate numbers of meteoroid impacts with the atmosphere per year based on Eq. 2.

Diameter, cm	No. of impacts per year
1	9.3×10^{12}
2	1.4×10^{12}
3	4.8×10^{11}
5	1.2×10^{11}
10	1.9×10^{10}

https://doi.org/10.5194/egusphere-2026-2921
Preprint. Discussion started: 8 July 2026

20	2.9×10^9
30	9.6×10^8
40	4.4×10^8
50	2.4×10^8
100 (1 m)	3.7×10^7

4 Meteor-derived dusty plasmoid hypothesis

The very strong correlation between observations of orbs with those of fireballs naturally leads to the hypothesis that orbs are derived from meteors in some way. What is left of an ablated meteor that terminates in the lower troposphere is a trail or cloud of dust that normally would be expected to be rapidly dispersed within the atmosphere. Meteoric dust contains a unique mix of extremely small, rapidly formed particles, many of which are ferromagnetic and weakly magnetized. The first-order explanation of orbs proposed here is based on the expected physical, chemical, electrical and magnetic properties of freshly formed meteoric dust in the lower atmosphere. The theory, based on the formation of a dusty plasma (Morfill and Ivlev, 2009; Merlino, 2021), naturally accounts for the plasma-like behaviour, but must also account for confinement, neutral buoyancy and emission of light for periods of up to one or more hours.

4.1 Meteors as sources of particulate matter

Iron meteoroids are almost entirely composed of an alloy of iron (~90-95%) and nickel (~5-10%) (Scott, 2020). It is the iron, and to a lesser extent nickel, that likely play the most important role in orb formation because both are ferromagnetic and both can release thermal energy through oxidation. For stony meteoroids (chondrites), which are the most common source of meteors, components include silicate minerals such as olivine and pyroxene and smaller amounts of iron, nickel and sulphide minerals, while carbonaceous chondrites also contain water and carbon (Abreu and Brearley, 2011). Even chondrites contain up to ~20% of iron and nickel, depending on type (Maksimova and Oshtrakh, 2019). Because of their high velocities of tens of km/s, meteor impacts with the atmosphere initially provide an enormous source of energy. Meteor entry velocities are in the range 11-72 km/s, such that a 1-kg meteor has an initial kinetic energy in the range 61 MJ to 2.6 GJ. Depending on composition, velocity and angle of impact, meteoroids of up to several cm in diameter are completely vaporized as they transit the atmosphere and form a fireball. As the fireball cools, vaporized silica, iron, nickel and other components condense to form nanometre-sized particles (Hervig et al., 2017, Saunders and Plane, 2006).

Vaporized metals react with oxygen at the high temperature of the fireball (~3,000-5,000 °C) to form oxides. Important to the theory presented here are the mixed oxidation state material magnetite (Fe_3O_4) and maghemite (γ-Fe_2O_3). Metallic iron and nickel are ferromagnetic, while magnetite (Fe_3O_4) and maghemite (γ-Fe_2O_3), both commonly reported in meteoritic dust, are ferrimagnetic, while ordinary α-Fe_2O_3 exhibits weak parasitic ferromagnetism at ambient temperature due to spin canting (Cornell and Schwertmann, 2003). As particles formed in

https://doi.org/10.5194/egusphere-2026-2921
Preprint. Discussion started: 8 July 2026

fireballs cool below their respective Curie temperatures (770°C for Fe, 358°C for Ni, 583°C for magnetite and 617°C for maghemite) (Dunlop and Özdemir 1997; Cornell and Schwertmann, 2003), any aligned magnetic dipole orientations can become locked in as remanent (permanent) magnetization, forming permanent nanoscale magnets. Although the Earth's magnetic field is relatively weak, ferromagnetic meteoritic particles commonly exhibit strong remanent magnetization. Rapid quenching of iron- and nickel-rich particles through their Curie temperatures in the presence of terrestrial and plasma-generated magnetic fields during meteor entry may plausibly contribute to the formation of remanent magnetic moments, consistent with the strong magnetic response observed in collected meteoritic dust (Suavet et al., 2009; Rochette et al., 2009). Such remanent magnetization provides a natural restoring force capable of contributing to confinement of a weakly charged dusty plasma. For the theory advanced here, only particles having magnetic properties, such as particles containing metallic iron and nickel, magnetite, maghemite and NiO (superparamagnetic for particles less than ~100-nm in diameter) are expected to be retained by the orb.

4.2 Magnetic self-assembly and confinement

Without a restoring force, both neutral and charged particles remaining after termination of a meteor in the atmosphere would rapidly disperse through atmospheric mixing, gravitational settling, turbulence, and electrostatic repulsion among similarly charged particles. In laboratory plasmas, confinement requires extremely strong externally applied magnetic fields; however, the magnetic fields associated with the motions of charged particles alone are orders of magnitude too weak to confine a plasma in the free atmosphere for more than a few seconds, similar to limitations identified in some models of ball lightning (Seward et al., 2001; Shmatov and Stephan, 2019). Instead, for orbs we propose that the restoring force arises from remanent magnetization of the condensed particles themselves. This provides a means of confining both charged and neutral particles provided that the particles possess sufficiently large remanent magnetic moments relative to thermal and aerodynamic disruptive forces.

Magnetized particles will align head-to-tail through dipole-dipole interactions and tend to form long chains. Those chains readily pair up lengthwise with other chains and crosslink through weaker through weaker multiparticle magnetic interaction such as dipole-induced dipole interactions, likely forming a dendritic scaffold, as illustrated schematically in Fig. 5. But if the magnetic forces are relatively weak, on the order of a few kT, where k is the Boltzmann constant, the bonds will frequently break and reform, resulting in a dynamically changing scaffolding. For two identical touching magnetic spheres of the same size, the head-to-tail dipole interaction energy is approximately:

$$U \approx \frac{\mu_0}{4\pi}\frac{2m^2}{r^3} \tag{3}$$

where μ_0 is the vacuum permeability (magnetic constant, $\mu_0 = 1.26 \times 10^{-6}\, N \cdot A^{-2}$), r is the interparticle distance given as $2a$ where a is the particle radius, and m is the magnetic moment, which is related to the magnetization M by $m = MV$ where V is the volume of a spherical particle with radius a.

https://doi.org/10.5194/egusphere-2026-2921
Preprint. Discussion started: 8 July 2026

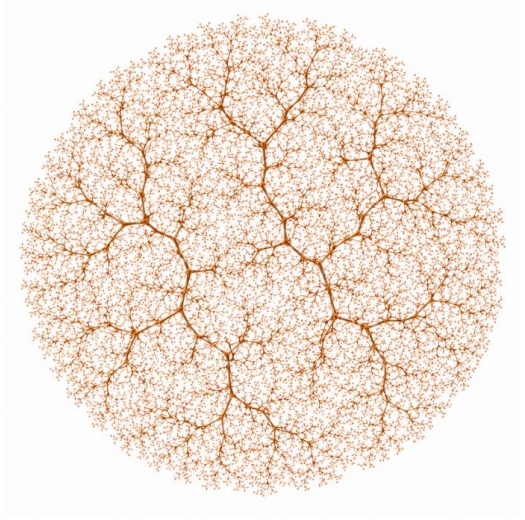

Fig. 5. Schematic representation of a 3-dimensional dendritic network of magnetic particles formed principally from dipole-dipole and dipole-induced dipole interactions. Because of weak magnetic energies of attraction of the order of only a few kT, it is expected that the network would be dynamic, constantly changing due to breaking of particle-particle bonds in the presence of uneven heating and convective heat transfer resulting from combustion of particles making up the structure.

Dividing by the characteristic thermal energy $\boldsymbol{kT}$, substituting for $\boldsymbol{r}$, $\boldsymbol{m}$, and $\boldsymbol{V}$, and rearranging we have the ratio of magnetic interaction energy to thermal kinetic energy as:

$$\frac{U}{kT} \approx \frac{\pi \mu_0 a^3}{9kT} M^2 \tag{4}$$

where U is the dipole-dipole bond energy and M is the magnetization. For a temperature of 300 K, values of U in the range kT to $5kT$ require approximate remanent magnetizations of 2.7×10^5 to 6.1×10^5 A m^{-1} for 10-nm diameter particles and 4.2×10^4 to 9.4×10^4 A m^{-1} for 35 nm particles.

Measurements of natural remanent magnetization (NRM) in meteorites span a wide range, typically corresponding to bulk magnetizations of order 10^{-1} to 10^3 A m^{-1}(Dunlop and Özdemir, 1997; Rochette et al., 2003; Gattacceca et al., 2004; Rochette et al., 2009). However, this bulk remanence is carried by a relatively small fraction of strongly magnetic particles, such as metallic Fe and Ni, the Fe-Ni alloy tetrataenite, and magnetite. Although bulk meteorite remanence is much smaller, individual particles can possess intrinsic magnetizations in the range 10^4 to 10^6 A m^{-1}, depending on composition, particle size, and thermal history. For meteors inducing very strong magnetization, particles will likely clump together and rapidly fall out of the atmosphere, while the particles of those of very weak magnetization would rapidly disperse. Some fraction of meteors rich in iron plausibly produce submicron meteoritic dust particles with magnetization values in the range of 10^4–10^6 A m^{-1}, placing magnetic dipole interaction energies in the range of a few kT and enabling dynamic, reversible aggregation to form a dendritic network resembling that of Fig. 5. Whether such weakly bonded aggregates can persist in the presence of atmospheric turbulence and convective motion remains uncertain and likely depends on continual restructuring and re-aggregation. If so, long-lived orbs would be expected to occur preferentially under relatively stable atmospheric conditions, such as within the nocturnal boundary layer.

https://doi.org/10.5194/egusphere-2026-2921
Preprint. Discussion started: 8 July 2026

4.3 Energy requirement and source

Orbs must produce enough energy to power its light emission and provide buoyancy. Like a hot air balloon, an orb requires generation of heat to reduce the density of its internal gas to offset the weight of the particulate matter it contains. As shown below, buoyancy requires on the order of ~400–2,000 W of power or a total energy of ~1.4–7.2 MJ for an orb that persists for an hour. Simple calculations readily show that this amount of energy greatly exceeds what could be available as energy stored as coulombic charge acquired during atmospheric entry or as power derived from Earth's electric field. Although some amount of tribocharging, proposed below for creating microdischarges and plasma-like behaviour, could be derived from the mechanical energy of the atmosphere such as wind shear and turbulence, this source also is much too weak, especially within the nocturnal boundary layer, to make a significant contribution. What is needed is a highly concentrated, continuous source of energy that slowly dissipates over a period of up to an hour or more. The magnitude of energy required almost certainly requires a chemical source.

The high temperature of the fireball might be expected to cause nearly complete oxidation of the silicon, carbon, iron, nickel and other trace components of the meteoroid. However, considering the very short entry time, typically a fraction of a second, some regions of the fireball could become depleted in oxygen, thereby preventing complete oxidation, or, more likely, elemental iron and nickel particles could be protected from complete oxidation by formation of a surface oxide layer. Iron–nickel particles are found in micrometeorites and meteoric dust collected at the Earth's surface, including surviving Fe–Ni metal particles and alloys such as kamacite and taenite (Genge et al., 2008; Van Maldeghem et al., 2023). Atmospheric entry commonly oxidizes smaller particles, producing iron oxide-rich cosmic spherules (Taylor et al., 1998). Nanoparticles of elemental iron and nickel oxidize rapidly in air at ambient temperature; sufficiently fine powders can be pyrophoric and may spontaneously ignite upon exposure to oxygen (Giri et al., 2001; Cornell et al., 2003; Alymov et al., 2017a; Alymov et al., 2017b). Iron oxidation provides a natural energy source for an orb, since particles containing magnetized Fe and Ni would contribute both to the dendritic orb structure rather than be lost due to diffusion and convection, while other reduced materials such as graphitic carbon or partially oxidized silica would be lost. The oxidation of elemental iron and nickel are both highly exothermic,

$$\mathrm{Fe} + \tfrac{3}{4}\,\mathrm{O_2} \rightarrow \tfrac{1}{2}\,\mathrm{Fe_2O_3}, \qquad \Delta H = -824\ \mathrm{kJ/mol\ or\ 14.8\ kJ/g} \tag{R1}$$

$$\mathrm{Ni} + \tfrac{1}{2}\mathrm{O_2} \rightarrow \mathrm{NiO}, \qquad \Delta H = -239\ \mathrm{kJ/mol\ or\ 4.07\ kJ/g} \tag{R2}$$

with iron being ~3.5 times more exothermic in its oxidation on both a molar and weight basis since Fe and Ni have similar atomic weights. For a Fe:Ni percent ratio of 90:10, the mix would provide an energy source of 13.7 kJ/g or 3.8 W/g if uniformly released over a period of 1 hour. For an energy requirement of 1.4-7.2 MJ, ~100-525 g of material would be required. For the estimates that follow, we will assume a range of 100-500 g. For a weighted density of 8.0 g/cm^3, this corresponds to the impact of an iron-nickel spherical meteoroid of diameter 2.9-4.9 cm. Iron meteoroids in this size range can, depending on velocity and entry angle, penetrate the atmosphere to the level of the troposphere. Stony meteoroids of this size are more likely to undergo extensive ablation and not penetrate to the troposphere. Of course, the iron and nickel meteoric dust forming an orb could comprise a small fraction of a much larger iron, stony or other meteor type. Also, a larger meteoroid could produce multiple orbs along its entry path.

https://doi.org/10.5194/egusphere-2026-2921
Preprint. Discussion started: 8 July 2026

Other weakly magnetic or nonmagnetic meteoritic components, such as silica, elemental carbon, and hematite formed during iron oxidation, would tend to be preferentially lost from the orb through diffusion, convection, and gravitational settling. In contrast, strongly magnetic phases such as metallic iron and nickel, along with the ferrimagnetic iron oxides magnetite and maghemite, would be preferentially retained within the aggregate. In addition to being removed by diffusion and convection, newly formed meteoric dust particles within a meteor trail might undergo magnetic flocculation (Luo and Nguyen, 2017) where particles with magnetic properties coalesce to form larger particles that settle faster than the non-magnetic ones, thereby separating the particles having magnetic properties from those that do not.

Possible evidence for orbs containing large quantities of iron is provided by the Council Bluffs, Iowa incident of 17 December 1977 (Vallée, 1992; Sturrock, 1999; Nolan et al., 2022). Numerous eyewitnesses observed a red luminous mass descend to the ground in Big Lake Park at approximately 19:45 CST (0145 GMT), while other witnesses reported a hovering red luminous object in the same area shortly beforehand. One observer described it as "a big round thing hovering in the sky, below treetops. It was hovering. It wasn't moving." Police and fire personnel arrived within approximately 15 minutes and observed a molten mass, estimated at 35–55 lb (16–25 kg), covering an area of roughly 4 × 6 ft and "running, boiling down to the edges of the levee." Chemical analyses conducted at Iowa State University and Griffin Pipe Products Company found the material to consist primarily of iron with only trace amounts of nickel and chromium. More recently, Nolan et al. (2022) re-examined surviving samples using modern secondary ion mass spectrometry and found isotopic ratios for Na, Mg, Al, Si, Ti, Cr and Fe to be consistent with terrestrial values. A terrestrial isotopic composition and low nickel abundance are consistent with iron derived from anthropogenic sources—for example re-entry of an iron booster rocket. In any case, the Council Bluffs event is noteworthy because it links eyewitness reports of a hovering luminous orb with the deposition of a large quantity of molten iron.

4.4 Buoyancy

The vast majority, more than 99%, of the energy expended by the orb ultimately is expended as heat. That heat provides a useful purpose, however, of providing buoyancy. To satisfy the observation that orbs tend to descend and stabilize at some altitude, the orb must be mostly air at elevated temperature to offset the weight of the retained meteor mass. The temperature required for neutral buoyancy is given by

$$\Delta T = T_{air}\frac{m}{\rho_{air}V - m} = T_{air}\frac{m}{\rho_{air}\left(\frac{\pi D^3}{6}\right) - m} \quad (5)$$

where ΔT is the required incremental temperature of the orb compared to the ambient temperature T_{air} (e.g., ~285 K), m is the mass of meteoric dust particles, ρ_{air} is the density of air (1.225 kg/m^3 at sea level), and V is the volume of the orb. Table 3 shows the elevated temperatures, ΔT, required to produce buoyancy for a range of combinations of total particulate mass and orb diameter.

https://doi.org/10.5194/egusphere-2026-2921
Preprint. Discussion started: 8 July 2026

Table 3. ΔT in units of °C required for buoyancy at an ambient temperature of 15°C and 100-m altitude.

Mass, g	Diameter, m				
	1.0	1.5	2.0	2.5	3.0
100	54	14	5.8	3.0	1.7
150	90	21	8.9	4.5	2.6
200	134	30	11	6.0	3.4
250	190	38	15	7.5	4.3
300	263	47	18	9.1	5.2
350	362	56	21	10	6.1
400	504	67	24	12	7.0
450	726	77	28	13	7.8
500	1,122	88	31	15	8.7

Next, we need to estimate the rate of heat production (power) required to produce a given ΔT and thus amount of Fe/Ni required. The steady-state temperature reached for a given rate of Fe/Ni oxidation is determined by the balance between the power of heat production, P_{prod}, and heat loss due to both convective, P_{conv}, and radiative, P_{rad}, components:

$$P_{\text{prod}} = P_{\text{conv}} + P_{\text{rad}} \tag{6}$$

The convective loss due to natural convection of a sphere is given by (see Appendix 1 for derivation)

$$P_{\text{conv}} = 3.7D^{1.75}\Delta T^{1.25} \tag{7}$$

where the diameter D is in metres, and thermal radiation loss is given by the black-body radiation law,

$$P_{\text{rad}} = \epsilon\sigma A_s[(T_a + \Delta T)^4 - T_a^4] \tag{8}$$

where ϵ is the emissivity, σ is the Steffan-Boltzmann constant and A_s is the exposed surface area of the dendritic, radiation-emitting structure. Thus, at steady state the total heat production power is equal to the sum of the losses due to convection and radiative loss,

$$P_{prod} = 3.7D^{1.75}\Delta T^{1.25} + \sigma A_p[(T_a + \Delta T)^4 - T_a^4] \tag{9}$$

where ΔT is the function of orb diameter and mass given by Eq. 5. The surface area A_p and emissivity ϵ of the particulate matter are highly uncertain. Initially formed meteoric particles are of the order of a few nanometres in diameter, but if confined to the volume of a 1-3 m diameter sphere, they would rapidly coagulate to form larger particles. For the model described above of a dendritic network, individual particles would naturally align along their dipoles into long chains, and those chains would tend to coalesce lengthwise into thicker chains. For simplification, if we consider the network as one long cylindrical filament cris-crossing the interior of the orb, the average filament diameter d_f the surface area is given by:

$$A_s = \frac{4m}{d_f\rho} \tag{10}$$

https://doi.org/10.5194/egusphere-2026-2921
Preprint. Discussion started: 8 July 2026

Results of calculations using equations 5 and 9 to determined required values of elevated temperature, ΔT, thermal power, P_{prod}, and iron/nickel mass to achieve neutral buoyancy are summarized graphically in Fig. 6. The calculations assume a radiative particle surface area of 0.25 m^2, or about 50% of the surface area of a 1-m sphere, and emissivity of 0.85, chosen as the bulk emissivity of a hematite surface coating. The assumed surface area implies an average filament diameter (Eq. 10) of ~200 µm, corresponding to a total length of ~10^5 m, sufficient to cris-cross a 1-m diameter of the sphere ~10^5 times. Still, the dendritic network would occupy only ~2.4% of the orb volume. Larger orbs can accommodate larger masses and/or thinner filaments.

Importantly, the requirement of orb buoyancy constrains the model to clumps of particles or filamentary aggregates having characteristic dimensions no greater than a few hundred microns in order to limit rapid radiative heat loss. A lower effective exposed surface area and/or emissivity permits buoyancy of smaller orbs. Also assumed in the calculations is that the average Fe/Ni oxidation rate corresponds to complete oxidation over a period of one hour, resulting in a mean power input of 3.4 W g^{-1}. More rapid oxidation would permit smaller but shorter-lived buoyant orbs. Sustained oxidation over periods approaching an hour would likely require that oxidation be limited by oxygen diffusion through oxide coatings and by the relatively small exposed surface area of the filamentary aggregate, with fresh reactive surfaces generated intermittently through continual restructuring within the orb. The filamentous morphology is therefore critical to the model, since it simultaneously limits radiative heat loss, moderates oxidation rates, and permits buoyancy at realistic power levels.

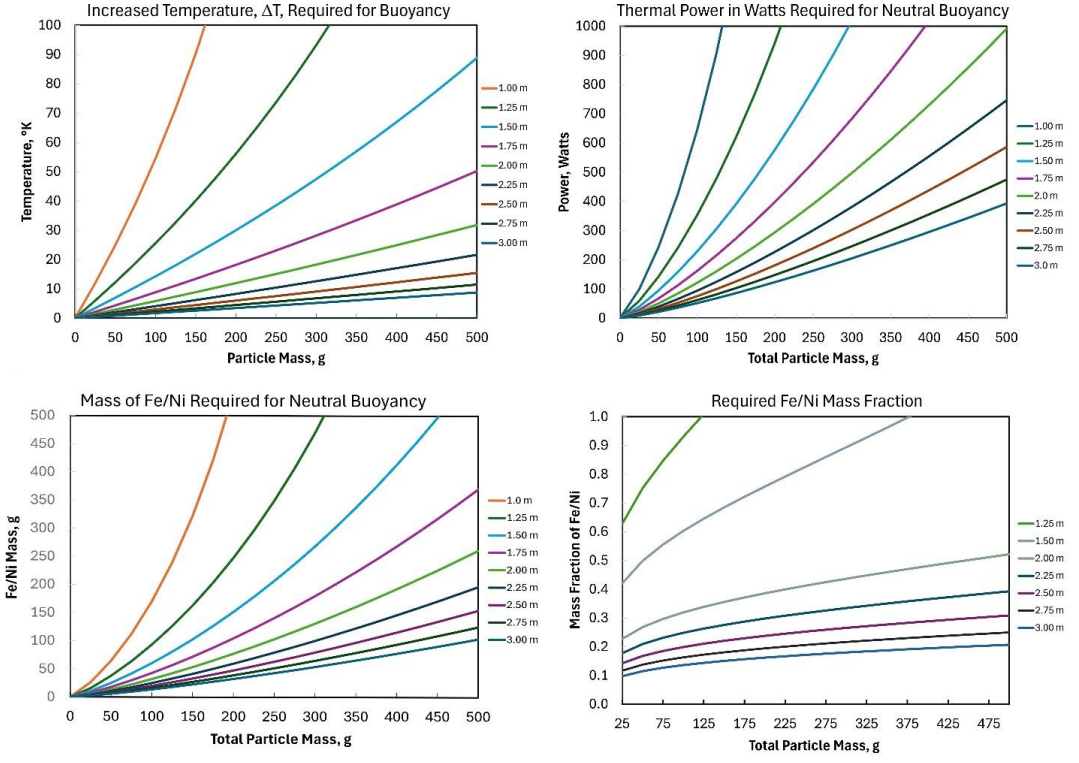

Fig. 6. Requirements for neutral buoyancy of an orb having diameters in the range 1 to 3 metres. Upper left: Temperature increase, ΔT in °C, required for neutral buoyancy as a function of total mass load for different of orb

https://doi.org/10.5194/egusphere-2026-2921
Preprint. Discussion started: 8 July 2026

diameters. Upper right: Thermal power in watts required for neutral buoyancy as a function of total mass load for different or diameters. Lower left: Mass of 90:10 Fe:Ni metal required to produce the power required for neutral buoyancy as a function of total mass load for `different orb diameters. Lower right: Fraction of total mass load that must be 90:10 Fe:Ni required for neutral buoyancy. Note that for parameters used in the calculation, a 1-m diameter orb cannot be made buoyant from Fe/Ni oxidation. Calculations assume particle surface area of 0.25 m^2, emissivity of 0.85 and that the Fe/Ni mix is completely oxidized at a uniform rate over a period of 1 hour.

For the assumed parameters, an orb diameter of at least 1.5 m is required to provide buoyancy for loads of ~100 g or more, and the orb needs to support more that the weight of the Fe:Ni fuel to produce the triboelectric effect described below. Smaller orbs may be possible if the convection and radiative emission terms are overestimated. For example, convective flow through the orb will oppose gravity, and drag on the orb's dendritic framework will produce drag, thus creating a upward force and the amount of mass that can be made buoyant. In any case, these calculations demonstrate plausibility of a buoyant orb in the 1-3 m diameter range derived from the components of meteoric dust alone.

4.5 Electrical activity

In order to explain the observed plasma-like behaviour of orbs, our model requires a method for producing electrical activity. We hypothesize that this is accomplished via conversion of mechanical energy to electrical energy through the triboelectric effect (Sotthewes et al., 2022; Pan and Zhang, 2019). Only a small fraction of the oxidation energy need be converted into mechanical agitation and triboelectric charging to sustain the weak electrical activity required for visible light emission. Although still not fully understood due to its complexity, electrostatic effects resulting from rubbing two dissimilar materials together have been known at least since the fifth century BC (Iverson and Lacks, 2012). Tribocharging of particles in wood processing plants, grain elevators, coal mines, flour mills and many other industrial facilities results in ignition of many fires and explosions annually (Hou et al., 2024; Tian et al., 2025), while electric field strengths in dust storms can result in lightning on both Earth (Swathi et al., 2025; Gangane et al., 2023) and Mars (Forget and Montabone, 2017). Tribocharging underlies lightning in thunderstorms and ash clouds of active volcanoes as well. Thus, tribocharging is common in the atmosphere.

Iron oxide nanoparticles have been widely investigated as active components in triboelectric nanogenerators (TENGs), demonstrating their ability to participate efficiently in charge transfer when paired with dissimilar materials (Im and Park, 2018; Vivekananthan et al., 2019; Khandelwal et al., 2021; Chakraborty et al., 2021; dos Reis et al., 2024; Kulandaivel et al., 2025). Tribocharging also occurs between particles of the same material due to differences in size, impurities, surface states, crystal defects, and other properties (Lowell et al., 1986a; Lowell et al. 1986b; Lacks et al., 2019). In addition to particles with iron and nickel cores, more weakly bound hematite, maghemite and nickel oxide are expected to be present in the orb, and all particles are expected to have large numbers of defects in their crystal structure due to their extremely rapid formation. In addition, slow or intermittent exothermic oxidation of oxide-coated metallic particles embedded within the dendritic structure, potentially aided by localized microdischarges, may continuously generate or release nanoparticles of hematite, magnetite, maghemite, and nickel oxide. These particles may move through voids and channels within the lattice, colliding with other particles and repeatedly making and breaking contact with the structure itself. Continual restructuring of the weakly bonded dendritic framework may further enhance contact electrification by increasing collision frequencies and exposing fresh

https://doi.org/10.5194/egusphere-2026-2921
Preprint. Discussion started: 8 July 2026

reactive and defect-rich surfaces. Although direct experimental confirmation is lacking, these mechanisms are qualitatively consistent with known dependencies of tribocharging on collision frequency, contact area, and impact energy. A proposed mechanism for triboelectric charging that results in microdischarges and a corona is illustrated in Fig. 7. Because the dendritic scaffold contains metallic iron cores connected through intermittent oxide-coated contacts, it is expected to possess weak electrical conductivity. Finite conductivity within the scaffold would allow triboelectrically generated charge to redistribute over local regions of the lattice, concentrating electric fields at protrusions, asperities, and gaps near the orb boundary where electrical breakdown is most favourable. There need not be fixed electrodes; instead, charge separation is distributed over many sites, with transient micro-cathodes and micro-anodes (localized electron emission and collection sites) forming dynamically. These sites are associated with scaffold features such as branch points, particle clumps, gaps, and surface asperities, where local electric fields are enhanced. Charge accumulation is expected to be enhanced at high-curvature regions, promoting electron emission into the surrounding air and initiating microdischarges.

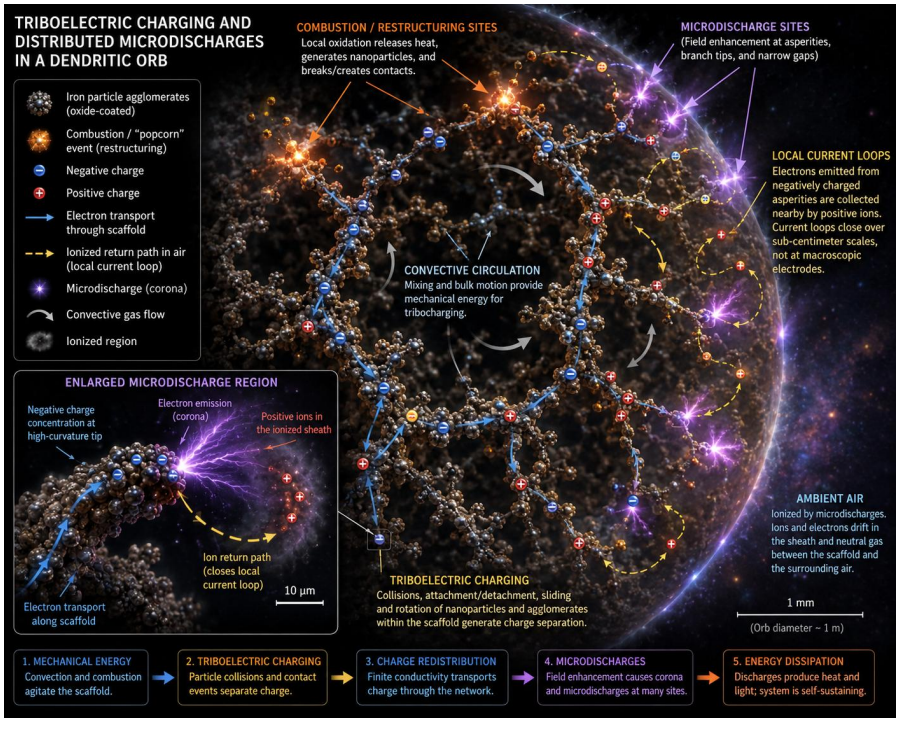

Fig. 7: Schematic illustration of triboelectric charging and distributed microdischarge processes within a dendritic meteoritic particle aggregate. Convective motion and intermittent combustion restructure the weakly conducting scaffold, producing triboelectric charge separation. Charge redistribution through the near-percolating filamentary network concentrates electric fields at asperities and narrow gaps, where localized corona microdischarges occur. Current loops are closed locally through ionized conduction paths in the surrounding air rather than through fixed macroscopic electrodes.

https://doi.org/10.5194/egusphere-2026-2921
Preprint. Discussion started: 8 July 2026

Charge neutrality is maintained locally, with electrons emitted into the surrounding sheath returning through short-range ionized conduction paths and recombination processes, while the metal-rich filamentary scaffold may act as a distributed, resistive pathway for charge transport, complementing ionized conduction in the surrounding air. Because charge transport occurs through a percolating network of semiconducting particles and intermittent contacts, the scaffold need not be highly conductive; it need only supply the small local currents required at many microdischarge sites. The finite resistance may be beneficial, because it limits runaway discharge and favours a spatially distributed corona rather than a single arc, analogous to resistive electrodes in dielectric-barrier corona discharge systems.

Once initiated, a weakly ionized corona can facilitate continued electrical activity by increasing the local charge-carrier density and conductivity, supplying ions and free electrons that facilitate subsequent microdischarges, and reshaping the electric field through space-charge effects that localize breakdown to microdischarges within the corona. The orb may be viewed analogously to a distributed capacitor weakly and locally coupled to the surrounding air through resistive, nonlinear discharge pathways. Electrical energy is not stored for long periods but is continuously regenerated by convective and mechanical agitation of the particles.

Everyday triboelectric charging phenomena, such as electrostatic discharge after walking across synthetic carpeting, demonstrate that frictional charging can generate electric field strengths (~30 kV/cm) sufficient for electrical breakdown in air. Breakdown to initiate a corona discharge is determined not by the average electric field strength across the orb, but by highly localized electric fields near surface asperities, sharp particle contacts, filament tips, and narrow gaps within the dendritic scaffold. Because the local electric field scales approximately as $E_{\mathrm{local}} \sim V/r$, where r is the local radius of curvature, micron- and submicron-scale protrusions can amplify modest potentials into electric fields sufficient for localized corona onset. Thus, even relatively small charge separations distributed across the scaffold may produce transient microdischarges at geometrically enhanced emission sites without requiring large-scale macroscopic voltages across the entire orb.

As discussed earlier, nanoparticles are especially effective at tribocharging, motivating their widespread use in triboelectric generators. Although the absolute charge carried by an individual particle decreases with surface area, the number of particles produced from a given meteoroid mass scales as the inverse cube of particle diameter. Consequently, reducing particle size from the micrometre to nanometre scale increases the total rate of particle–particle contacts and near-contact interactions by up to three orders of magnitude, resulting in large increases in electrical current.

Order-of-magnitude estimates demonstrate that the required electrical throughput is modest on a per-particle basis. For a 1-m-diameter orb radiating ~0.2 W of visible light, the associated electrical power requirement is plausibly only a few to perhaps a few tens of watts. At effective discharge potentials of 1–10 kV, 10 W corresponds to currents of only ~1–10 mA. For a representative case in which a 4-cm iron–nickel meteoroid of density ~8 g cm^{-3} is converted into 10–100 nm particles, the resulting particulate population would contain roughly 10^{15}–10^{18} particles depending on particle size. If only ~1% of those particles actively participate in charge cycling at any given time, the required electron transfer rate is of the order of only ~0.1–10 electrons s^{-1} per active particle. Such rates are well within the range implied by known aerosol charging, flow electrification, and dust-storm electrification phenomena, particularly

https://doi.org/10.5194/egusphere-2026-2921
Preprint. Discussion started: 8 July 2026

in environments where weak ionization and microdischarges continually replenish charge carriers (Kok and Lacks, 2009; Forward et al., 2009).

Taken together, these processes describe a self-organized, dynamically sustained system in which magnetic interactions structure the particulate cloud, triboelectric charging continuously generates electrical energy, and distributed microdischarges provide a pathway for its dissipation as heat and light – all driven by energy derived from iron and nickel oxidation.

5 Origins of visible light emissions

Assuming that orbs have a brightness at least equal to that of the planet Venus when viewed at a distance of 1 km, we estimate that the minimal orb light emission power must be of the order ~0.16 W, calculated as follows. At its maximum brightness, Venus has an apparent magnitude of -4.9, corresponding to 1.25×10^{-8} W/m^2 arriving at the observer's eye. The radiant power of a spherical source required at distance r of 1 km to produce the same light intensity is 1.25×10^{-8} W/m^2 $\times 4\pi r^2 = 0.16$ W. As discussed above, metallic iron and nickel oxidation provide up to a few hundred watts of power. Only a tiny fraction, of the order of 0.1% of this energy, must be converted to visible light, but by what mechanism? Possibilities include (1) electrical discharge, (2) high-temperature combustion and (3) chemiluminescence.

Microdischarges, which appear to be present in some videos and images, excite molecular nitrogen in the surrounding air, generating the observed bluish-white emissions from the second positive system of nitrogen ($C^3\Pi_u \rightarrow B^3\Pi g$) in the 350-450 nm wavelength range typical of discharges in air. Other colours of light may originate from excitation of metal atoms and their ions, especially Fe (yellow-orange), Ni (pale green, blue-white), K (violet), Na (yellow), Ca (red, orange) and Mg (blue-green). Absorbance of emissions within the orb, especially by iron oxides, could contribute to the orange and red colours of many orbs.

Although the orb filaments are likely hundreds of microns thick (in order to reduce radiative cooling and provide buoyancy), it is expected to be made up of clusters of nanoparticles, most of which have cores of iron and nickel. Being pyrophoric, these may produce continuous or bursts of light characteristic of Fe, Ni and various impurities such as K, Na, Ca and Mg. The extremely high local temperature of the discharge itself may induce the combustion of metal particles that are otherwise slow reacting due to their oxide coating, and micron-sized particles made of oxide-coated metal particles may be combusted simultaneously, resulting in even higher local temperatures. Thus, incandescence of particles heated by microdischarges and metal combustion may contribute to the commonly observed white, orange and red emissions as well.

Persistent afterglows of varying colour along meteor trajectories, known as "trains", can last from minutes to hours and have been documented for more than a millennium (Beech, 1987). These phenomena, however, occur primarily in the mesosphere and thermosphere, where low ambient pressure and correspondingly low collisional quenching rates permit efficient chemiluminescence. At such altitudes, reactions involving NO, O atoms, and O_3 — analogous in some respects to auroral processes — can produce visible green, red, and near-infrared light. Although electrical discharges in air also generate NO, O, and O_3, these chemiluminescent pathways are unlikely to contribute

https://doi.org/10.5194/egusphere-2026-2921
Preprint. Discussion started: 8 July 2026

significantly to orb emission in the lower atmosphere. At tropospheric pressures, rapid three-body recombination of O atoms to form O_3 and efficient collisional quenching of electronically excited NO_2 strongly suppress radiative emission due to pressure being orders of magnitude higher than in the mesosphere and thermosphere. As a result, such reactions cannot account for the observed brightness and persistence of orb emissions in the lower atmosphere. These considerations instead point to high-energy electronic excitation associated with localized plasma formation, distributed microdischarges, and possibly localized Fe/Ni combustion processes as the dominant sources of visible light emission in orbs.

In summary, the model predicts that optical spectra of orbs should exhibit a combination of molecular nitrogen emission bands, metallic line emission, and broadband thermal continuum emission varying spatially and temporally across the orb. It would therefore be especially useful to obtain optical emission spectra of orbs to identify the emitting species. This could be accomplished using methods common in amateur astronomy, in which a diffraction grating is positioned in front of a camera lens, thereby simultaneously recording both an image of the orb and its visible spectrum. Spectroscopic observations of iron, silicon, and calcium emission lines in luminous phenomena identified as ball lightning have proven particularly useful in constraining models of that related phenomenon (Cen et al., 2014), which, although different from orbs in many respects, may also involve dusty plasma processes associated with iron-bearing particles generated by vaporization of soil during lightning strikes.

6 Orb strength and lifespan

Figure 6 shows an orb observed near ground level that was reported to approach a tree, appear to make contact with the upper branches, and then retreat and hover (NUFORC, report 193124). A video recorded during the subsequent hovering stage shows ongoing discharges with multicoloured emissions, while the internal plasma glow is greatly diminished. Under these conditions, a structured, globular mass becomes visible, proposed here to consist of an aggregate of meteoric dust particles. Such behaviour suggests an energy-depleted orb in which sustained triboelectric charging and microdischarge activity have weakened. Consistent with the theory presented here, as the metallic iron fuel becomes depleted, reduced heating diminishes buoyancy, causing the orb to sink to lower altitudes. Ultimately, descent may culminate in discharge to a grounded object at the surface, followed by dissipation and deposition of particulate material. Orb lifetimes of minutes to hours would be dependent on factors like particle composition, size distribution, degree of magnetization and meteorological conditions.

https://doi.org/10.5194/egusphere-2026-2921
Preprint. Discussion started: 8 July 2026

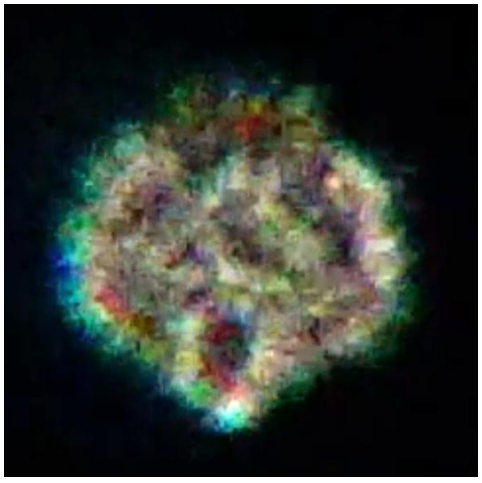

Fig. 8: Frame captured from the video posted with NUFORC report 193124 showing the internal structure of a near-ground-level orb showing white, green and red emissions. The underexposed mage has been brightened by 50% to bring out more detail. The active discharge into air at the surface is best viewed in the video.

7 Conclusions

The iron-based, dusty plasma model presented here plausibly explains many reported features of luminous orbs: buoyancy, long lifetimes of minutes to hours, electrical behaviour and pronounced colour variability. Importantly, the model does not require large reservoirs of stored electrostatic energy or global ionization; instead, luminosity is sustained through continuous, distributed energy conversion through tribocharging driven by convection induced by iron oxidation. As such, it provides a physically grounded mechanism by which a weakly ionized dusty plasma can remain luminous and dynamically active for extended periods of time.

Because electrical breakdown is threshold-dependent, modest fluctuations in pressure, humidity, particle concentration, or local electric field strength could lead to intermittent discharge behaviour, producing the observed blinking and flickering of orbs. Weakly charged orbs must accumulate additional charge before re-initiating discharge, while more strongly charged orbs can perturb the local electric field sufficiently to induce emission in nearby non-emitting or weakly emitting orbs, consistent with reports of “dark” orbs becoming luminous in the presence of active ones. A magnetically confined dusty plasma also provides a plausible explanation for orb division and merging. Weak inter-orb binding mediated by charge-induced dipole and higher-order multipole interactions would be expected, analogous to van der Waals forces between molecules, and could result in merging. From an energetic perspective, there may exist preferred orb sizes for given combinations of mass, particle size, charge state, and magnetic strength, such that under some conditions favour splitting into two or more orbs under mechanical stresses from wind shear or turbulence. Orb division resulting in orbs of different colours may result from partial phase separation during splitting, yielding separate orb fragments with differing particle compositions or size distributions. Also, mutual electrostatic repulsion would tend to drive smaller particles toward the aggregate periphery, while larger particles remain preferentially concentrated toward the interior, making asymmetric partitioning during division likely. Because

https://doi.org/10.5194/egusphere-2026-2921
Preprint. Discussion started: 8 July 2026

smaller particles are more efficient triboelectric generators, these asymmetries could naturally produce differences in discharge energy and emission wavelengths among the resulting orbs.

Here, we argue that luminous orbs represent a rare but physically real atmospheric phenomenon. Any model capable of addressing their origin, containment, fluidity, buoyancy, plasma-like behaviour, energy source, and light emission is necessarily unconventional. However, the strong correlation between orb observations and meteor activity reported here provides a solid physical starting point. Although novel in several respects, the proposed framework is based on established physical principles, and its components are testable through laboratory experiments, targeted atmospheric measurements, and more detailed theoretical modelling. It may even be possible to generate orbs in the laboratory from magnetic nanoparticles of iron.

Although only nocturnal, luminous orbs are considered here, it is important to note that such objects would likely appear very different under daylight conditions. Because sunlight is many orders of magnitude brighter than the visible emission from an orb, self-luminosity would be largely obscured. At the metal and metal-oxide particle concentrations considered above, the orb would be optically thick despite particles occupying only a small fraction of the total volume. Consequently, during daylight an orb would likely appear as an opaque object rather than a luminous one, with a white, gray, or silvery appearance depending on illumination, viewing angle, and particle composition. The apparent shape of an orb would also depend on atmospheric conditions and internal dynamics. While a quiescent orb might appear approximately spherical, internal convection, rotation, deformation by ambient winds, and variations in particle concentration could produce a range of morphologies, including spherical, lenticular (disc-like), and elongated or cigar-shaped forms, and those forms could vary over time (shape shift). Such appearances are broadly consistent with several commonly reported classes of UAP observations.

In addition to scientific interest, orbs have acquired substantial popular culture significance. Providing a physics-based explanation has the potential to resolve a large fraction of reported UAP sightings and reduce public anxiety associated with these rare and poorly understood events. Orbs are routinely reported by civilian and military pilots and may constitute an air traffic hazard. Also, orbs could be an unrecognized ignition source for wildfires, especially in grasslands. Since orbs occur on Earth, similar phenomena almost certainly occur on other planets having atmospheres, making further study of this interesting phenomenon highly relevant to planetary and space science as well.

Data Availability: All data referenced in this work are available on the NUFORC and AMS public websites.

Competing Interests: The author declares that he has no conflict of interest.

Acknowledgments: This work was made possible by data collected by the National UFO Reporting Center founded in 1974 by Robert J. Gribble. We especially thank Peter Davenport and Christian Stepien of NUFORC for their assistance and permission to use orb images. The AI assistant ChatGPT was used as an interactive tool throughout this research, assisting in derivation of equations, feasibility calculations, analysis of images, creation of Figs. 5 and 7, bibliographic searches and text editing.

https://doi.org/10.5194/egusphere-2026-2921
Preprint. Discussion started: 8 July 2026

References

Abreu, N. M. and Brearley, J. M.: Deciphering the nebular and asteroidal record of silicates and organic material in matrix of the reduced CV3 chondrite Vigarano, Meteorit. Planet. Sci., 46, 252–274, https://doi.org/10.1111/j.1945-5100.2010.01149.x, 2011.

Aerospace Corporation: CORDS reentry database, available at: https://aerospace.org/reentries (last access: 15 May 2026), 2026.

Alymov, M. I., Rubtsov, N. M., Seplyarskii, B. S., Zelenskii, V. A., Ankudinov, A. B., Kovalev, I. D., Kochetkov, R. A., and Shchukin, A. S.: Passivation of iron nanopowders at temperatures below 0 °C in a dry air atmosphere, Doklady Chemistry, 477, 261–264, https://doi.org/10.1134/S0012500817110039, 2017a.

Alymov, M. I., Rubtsov, N. M., Seplyarskii, B. S., Zelenskii, V. A., Ankudinov, A. B., Kovalev, I. D., Kochetkov, R. A., and Shchukin, A. S.: Passivation of nickel nanoparticles at temperatures below 0 °C, Nanotechnologies in Russia, 12, 577–582, https://doi.org/10.1134/S1995078017060027, 2017b.

American Meteor Society: Fireball Reports, available at: https://fireball.amsmeteors.org/members/imo_view/browse_reports (last access: 15 May 2026), 2026.

Beech, M.: On the trail of meteor trains, Q. J. R. Astron. Soc., 28, 445–454, 1987.

Brown, P., Spalding, R. E., ReVelle, D. O., Tagliaferri, E., and Worden, S. P.: The flux of small near-Earth objects colliding with the Earth, Nature, 420, 294–296, https://doi.org/10.1038/nature01238, 2002.

Cen, J., Ping, Y., and Xue, S.: Observation of the optical spectral characteristics of ball lightning, Phys. Rev. Lett., 112, 035001, https://doi.org/10.1103/PhysRevLett.112.035001, 2014.

Chakraborty, I., Lai, S.-N., Wu, M.-C., Lin, H.-Y., Li, C., Wu, J. M., and Lai, C.-S.: Charge trapping with α-Fe_2O_3 nanoparticles accompanied by human hair towards an enriched triboelectric series and a sustainable circular bioeconomy, Mater. Horiz., 8, 3149–3159, https://doi.org/10.1039/D1MH00919B, 2021.

Cornell, R. M. and Schwertmann, U.: The Iron Oxides: Structure, Properties, Reactions, Occurrences and Uses, 2nd ed., Wiley-VCH, Weinheim, 2003.

dos Reis, G. S., de Oliveira, H. P., Candido, I. C. M., Freire, A. L., Molaiyan, P., Dotto, G. L., Grimm, A., and Mikkola, J. P.: Supercapacitors and triboelectric nanogenerators based on electrodes of greener iron nanoparticles/carbon nanotube composites, Sci. Rep., 14, 11555, https://doi.org/10.1038/s41598-024-61173-5, 2024.

Dunlop, D. J. and Özdemir, Ö.: Rock Magnetism: Fundamentals and Frontiers, Cambridge University Press, Cambridge, UK, 573 pp., https://doi.org/10.1017/CBO9780511612794, 1997.

Forget, F. and Montabone, L.: Atmospheric dust on Mars, in: Proceedings of the 47th Int. Conf. on Environmental Systems (ICES), Charleston, SC, USA, 16–20 July 2017, ICES-2017-175, 2017.

Forward, K. M., Lacks, D. J., and Sankaran, R. M.: Charge segregation depends on particle size in triboelectrically charged granular materials, Phys. Rev. Lett., 102, 028001, https://doi.org/10.1103/PhysRevLett.102.028001, 2009.

Gangane, A., Pawar, S. D., Gopalakrishnan, V., and Saikrishnan, K. C.: Effect of dust particles on lightning flash rate and polarity of dust storms over India, Nat. Hazards, 115, 2505–2529, https://doi.org/10.1007/s11069-022-05651-x, 2023.

https://doi.org/10.5194/egusphere-2026-2921
Preprint. Discussion started: 8 July 2026

Gattacceca, J., Rochette, P., Denise, M., Consolmagno, G., and Folco, L.: An impact origin for the hypervelocity carbonaceous chondrites from Antarctica supported by magnetic properties, Earth Planet. Sci. Lett., 227, 377–393, https://doi.org/10.1016/j.epsl.2004.08.002, 2004.

Genge, M. J., Engrand, C., Gounelle, M., and Taylor, S.: The classification of micrometeorites, Meteorit. Planet. Sci., 43, 497–515, https://doi.org/10.1111/j.1945-5100.2008.tb00668.x, 2008.

Giri, S., Samanta, S., Maji, S., Ganguli, S., Bhaumik, A., and Bhattacharya, D.: Surface oxidation of iron nanoparticles, Appl. Surf. Sci., 182, 345–350, https://doi.org/10.1016/S0169-4332(01)00446-9, 2001.

Hervig, M. E., Brooke, J. S. A., Feng, W., Bardeen, C. G., and Plane, J. M. C.: Constraints on meteoric smoke composition and meteoric influx using SOFIE observations with models, J. Geophys. Res.-Atmos., 122, 13495–13505, https://doi.org/10.1002/2017JD027657, 2017.

Hou, J., Hu, G., Grace, J. R., and Bi, X.: Experimental study of electrostatic charging related to prevention of fire and dust explosions in wood processing facilities, J. Electrost., 132, 103983, https://doi.org/10.1016/j.elstat.2024.103983, 2024.

Im, J.-S. and Park, I.-K.: Mechanically robust magnetic Fe_3O_4 nanoparticle/polyvinylidene fluoride composite nanofiber and its application in a triboelectric nanogenerator, ACS Appl. Mater. Interfaces, 10, 25660–25665, https://doi.org/10.1021/acsami.8b07621, 2018.

Iverson, P. and Lacks, D. J.: A life of its own: The tenuous connection between Thales of Miletus and the study of electrostatic charging, J. Electrost., 70, 309–311, https://doi.org/10.1016/j.elstat.2012.03.002, 2012.

Jenniskens, P.: Meteor stream activity. II. Meteor outbursts, Astron. Astrophys., 295, 206–235,1995.

Jenniskens, P., Nénon, Q., Albers, J., Gural, P. S., Haberman, B., Morales, R., Grigsby, B. J., Samuels, D., and Johannink, C.: The established meteor showers as observed by CAMS, Icarus, 266, 331–354, https://doi.org/10.1016/j.icarus.2015.09.013, 2016.

Joseph, R. G., Impey, C., Planchon, O., del Gaudio, R., Abu Safa, M., Sumanarathna, A. R., Ansbro, E., Bianciardi, G., Gibson, C. H., and Schild, R.: Extraterrestrial life in the thermosphere: plasmas, UAP, pre-life, fourth state of matter, J. Mod. Phys., 15, 322–374, doi: 10.4236/jmp.2024.153015 , 2024a.

Joseph, R. G., Impey, C., Planchon, O., Armstrong, R. A., Gibson, C. H., and Schild, R. E.: Unidentified anomalous phenomena, extraterrestrial life, plasmoids, shape shifters, replicons, thunderstorms, lightning, hallucinations, aircraft disasters, ocean sightings, J. Mod. Phys., 15, 1760–1868, https://doi.org/10.4236/jmp.2024.1511079, 2024a.

Joseph, R. G., Armstrong, R. A., Wolowski, K., Abu Safa, M., Dunne, M. C. M., del Gaudio, R. R., and Schild, R.: Plasmas: A fourth domain of life? RNA, DNA, consciousness and statistical analysis of "unidentified anomalous phenomena" in the thermosphere, J. Mod. Phys., 16, https://doi.org/10.4236/jmp.2025.169066 , 2025.

Khandelwal, G., Raj, N. P. M. J., and Kim, S.-J.: Materials beyond conventional triboelectric series for fabrication and applications of triboelectric nanogenerators, Adv. Energy Mater., 11, 2101170, https://doi.org/10.1002/aenm.202101170, 2021.

Kok, J. F. and Lacks, D. J.: Electrification of granular systems of identical insulating particles, Phys. Rev. E, 79, 051304, https://doi.org/10.1103/PhysRevE.79.051304, 2009.

Kulandaivel, A., Potu, S., Madathil, N., Velpula, M., Babu, A., Khanapuram, U. K., and Rajaboina, R. K.: Magnetite nanoparticles based triboelectric nanogenerators for self powering applications, J. Mater. Sci.-Mater. Electron., 36, 471, https://doi.org/10.1007/s10854-025-14422-w, 2025.

Lacks, D. J. and Shinbrot, T.: Long-standing and unresolved issues in triboelectric charging, Nat. Rev. Chem., 3, 465–476, https://doi.org/10.1038/s41570-019-0115-1, 2019.

https://doi.org/10.5194/egusphere-2026-2921
Preprint. Discussion started: 8 July 2026

Lowell, J. and Truscott, W. S.: Triboelectrification of identical insulators. I. An experimental investigation, J. Phys. D: Appl. Phys., 19, 1273–1280, https://doi.org/10.1088/0022-3727/19/7/014, 1986a.

Lowell, J. and Truscott, W. S.: Triboelectrification of identical insulators. II. Theory and further experiments, J. Phys. D: Appl. Phys., 19, 1281–1298, https://doi.org/10.1088/0022-3727/19/7/015, 1986b.

Luo, L. and Nguyen, V.: A review of principles and applications of magnetic flocculation to separate ultrafine magnetic particles, Sep. Purif. Technol., 172, 85–99, https://doi.org/10.1016/j.seppur.2016.07.021, 2017.

Maksimova, A. A. and Oshtrakh, M. I.: Ordinary chondrites: What can we learn using Mössbauer spectroscopy, J. Mol. Struct., 370, 12–22, https://doi.org/10.1016/j.molstruc.2019.02.024, 2019.
Morfill, G. E. and Ivlev, A. V.: Complex plasmas: An interdisciplinary research field, Rev. Mod. Phys., 81, 1353–1404, https://doi.org/10.1103/RevModPhys.81.1353, 2009.

Merlino, R., Dusty plasmas: from Saturn's rings to semiconductor processing devices, Adv. Phys.: X, 6, 1873859, https://doi.org/10.1080/23746149.2021.1873859, 2021.

National UFO Reporting Center: NUFORC database, available at: https://nuforc.org/ (last access: 15 May 2026), 2026.

Nolan, G. P., Vallée, J. F., Jiang, S., and Lemke, L. G.: Improved instrumental techniques, including isotopic analysis, applicable to the characterization of unusual materials with potential relevance to aerospace forensics, Prog. Aerosp. Sci., 128, 100788, https://doi.org/10.1016/j.paerosci.2021.100788, 2022.

N2YO: Genesis 2 experimental space habitat satellite tracking data, available at: https://www.n2yo.com/satellite/?s=31789 (last access: 15 May 2026), 2026.

Pan, S. and Zhang, Z.: Fundamental theories and basic principles of triboelectric effect: A review, Friction, 7, 2–17, https://doi.org/10.1007/s40544-018-0217-7, 2019.

Rendtel, J.: Meteoroid streams and meteor showers, J. Int. Meteor Organ., 42, 155–162, available at: https://www.researchgate.net/publication/272814104_Meteoroid_streams_meteor_showers (last access: 15 May 2026), 2014.

Rochette, P., Gattacceca, J., Bonal, L., Bourot-Denise, M., and Consolmagno, G.: Magnetic classification of stony meteorites: 1. Ordinary chondrites, Meteorit. Planet. Sci., 38, 251–268, https://doi.org/10.1111/j.1945-5100.2003.tb00261.x, 2003.

Rochette, P., Weiss, B. P., and Gattacceca, J.: Magnetism of extraterrestrial materials, Elements, 5, 223–228, https://doi.org/10.2113/gselements.5.4.223, 2009.

Saunders, R. W. and Plane, J. M. C.: A laboratory study of meteor smoke analogues: Composition, optical properties and growth kinetics, J. Atmos. Sol.-Terr. Phys., 68, 2182–2202, https://doi.org/10.1016/j.jastp.2006.09.006, 2006.

Seward, C., Chiping, C., and Ware, K.: Ball lightning explained as a stable plasma toroid, in: PPPS-2001 Pulsed Power Plasma Science 2001, 28th IEEE International Conference on Plasma Science and 13th IEEE International Pulsed Power Conference, Las Vegas, NV, USA, 17–22 June 2001, 269–272, vol. 1, https://doi.org/10.1109/PPC.2001.1002044, 2001.

Shamatov, M. L. and Stephan, K. D.: Advances in ball lightning research, J. Atmos. Sol.-Terr. Phys., 195, 105115, https://doi.org/10.1016/j.jastp.2019.105115, 2019.

Scott, E. R. D.: Iron meteorites: Composition, age, and origin, Oxford Research Encyclopedia of Planetary Science, https://doi.org/10.1093/acrefore/9780190647926.013.206, 2020.

https://doi.org/10.5194/egusphere-2026-2921
Preprint. Discussion started: 8 July 2026

Sotthewes, K., Gardeniers, H. J. G. E., Desmet, G., and Jimidar, I. S. M.: Triboelectric charging of particles, an ongoing matter: From the early onset of planet formation to assembling crystals, ACS Omega, 7, 41828–41839, https://doi.org/10.1021/acsomega.2c05629, 2022.

Sturrock, P. A.: The UFO Enigma: A New Review of the Physical Evidence, Warner Books, New York, NY, USA, 1999.

Suavet, C., Gattacceca, J., Rochette, P., Perchiazzi, N., Folco, L., Duprat, J., and Harvey, R. P.: Magnetic properties of micrometeorites, J. Geophys. Res.-Solid Earth, 114, B04102, https://doi.org/10.1029/2008JB005831, 2009.

Swathi, V. S., Panda, S. K., Mondal, U., and Sharma, D.: Investigating dust storm dynamics and lightning interactions using the Weather Research and Forecasting-Chemistry (WRF-Chem) model over India, Sci. Total Environ., 995, 180083, https://doi.org/10.1016/j.scitotenv.2025.180083, 2025.

Taylor, S., Lever, J. H., and Harvey, R. P.: Accretion rate of cosmic spherules measured at the South Pole, Nature, 392, 899–903, https://doi.org/10.1038/31850, 1998.

Tian, C., Yang, Z., and Zhang, L.: A review of grain dust explosions: Prevention and control, Results Eng., 26, 105483, https://doi.org/10.1016/j.rineng.2025.105483, 2025.

Van Maldeghem, F., Goderis, S., Soens, B., and Claeys, P.: Cosmic micrometeorites from deep-sea sediments: links to chondritic parent bodies and the effects of alteration, Geochim. Cosmochim. Acta, 342, 1–24, https://doi.org/10.1016/j.gca.2022.12.023, 2023.

Vallée, J. F.: UFO Chronicles of the Soviet Union: A Cosmic Samizdat, Ballantine Books, New York, NY, USA, 1992.

Vaubaillon, J., Colas, F., and Jorda, L.: A new method to predict meteor showers, Astron. Astrophys., 439, 761–770, https://doi.org/10.1051/0004-6361:20041544, 2005.

Vivekananthan, V., Chandrasekhar, A., Alluri, N. R., Purusothaman, Y., Khandelwal, G., Pandey, R., and Kim, S.-J.: Fe_2O_3 magnetic particles derived triboelectric-electromagnetic hybrid generator for zero-power consuming seismic detection, Nano Energy, 64, 103926, https://doi.org/10.1016/j.nanoen.2019.103926, 2019.

https://doi.org/10.5194/egusphere-2026-2921
Preprint. Discussion started: 8 July 2026

Appendix 1: Natural Convection Heat Transfer of a Sphere

Starting from the natural-convection sphere correlation:

$$P_{\text{conv}} = hA\Delta T \tag{A1}$$

with

$$A = \pi D^2 \tag{A2}$$

and

$$h = \frac{k_{\text{air}} Nu}{D} \tag{A3}$$

we have:

$$P_{\text{conv}} = \pi k_{\text{air}} D\, Nu\, \Delta T \tag{A4}$$

where $\Delta T = T_s - T_a$, the difference between the surface temperature ambient temperatures. For natural convection around a sphere, neglecting the small conduction-limit term $Nu = 2$,

$$Nu \approx C\, Ra^{1/4} \tag{A5}$$

where $C \approx 0.48$–0.59, depending on the Prandtl-number correction. The Rayleigh number is:

$$Ra = \frac{g\beta\Delta T D^3}{\nu\alpha} \tag{A6}$$

Substituting:

$$P_{\text{conv}} = \pi k_{\text{air}} D\Delta T C \left(\frac{g\beta\Delta T D^3}{\nu\alpha}\right)^{1/4} \tag{A7}$$

Collecting powers of D and ΔT,

$$P_{\text{conv}} = \pi k_{\text{air}} C \left(\frac{g\beta}{\nu\alpha}\right)^{1/4} D^{7/4}\Delta T^{5/4} \tag{A8}$$

and substituting values of constants we obtain:

$$P_{\text{conv}} = 3.7 D^{1.75}\Delta T^{1.25} \tag{A9}$$

for air near ambient temperature, with D in meters, ΔT in K, and P_{conv} in watts. This is an approximate natural-convection expression for a sphere in still air, valid for moderate temperature differences and ordinary atmospheric conditions.